ELSEVIER

Journal of Nuclear Materials 280 (2000) 285–294

journal of nuclear materials

www.elsevier.nl/locate/jnucmat

Thermal removal of gallium from gallia-doped ceria

Young Soo Park [a,*], Hong Yong Sohn [b], Darryl P. Butt [a,1]

[a] *Materials Science and Technology Division, Los Alamos National Laboratory, MS G755, Los Alamos, NM 87545, USA*
[b] *Department of Metallurgical Engineering, University of Utah, Salt Lake City, UT 84112, USA*

Received 1 February 2000; accepted 19 April 2000

Abstract

The potential for removing gallium from Ga-doped CeO_{2-x} by thermal means was studied for the purpose of assessing gallium removal from PuO_{2-x}. The latter is of interest to those considering the storage or use of weapon-grade Pu, for example as a mixed oxide fuel component. Experiments were done by varying temperature, gas composition, exposure time, sample size, particle size, and gas flow rate. The kinetics of gallium removal were assessed through measurements of weight change, scanning electron microscopy, and chemical analyses. Results suggest that the gallium level can be reduced significantly by thermal treatments in Ar–6% H_2. Gallium species segregate to grain boundaries because of the low solubility of Ga_2O_3 in CeO_2. The kinetics and microstructural observations suggest that both gaseous and solid-state diffusion of gallium species are important for the removal of gallium.

1. Introduction

It has been considered to use weapon-grade plutonium as reactor fuels for the peaceful production of electricity [1–3]. Unlike reactor-grade Pu, weapon-grade Pu may contain a minor amount of Ga (melting point: 29.8°C) added to stabilize the δ-phase and make it easily machinable. Gallium is known to degrade the properties of many metallic materials via corrosion, embrittlement, or intermetallic phase formation [4–8]. Thus, the gallium-induced corrosion of cladding materials as well as fuel sintering is a concern. For this reason, the gallium level should be reduced to less than 100 wppm before the weapon-grade plutonium oxide can be used as a fuel [5,21]. The PuO_2 powder will be blended with UO_2 in a ratio of 1:20, such that the resultant gallium concentration is reduced to below 5 wppm. The sub-oxide of gallium is also further volatilized and evolved during sintering of this mixture, so that the final concentration in fresh fuel will be on the order of a few wppm [5].

Due to the significant quantities of waste that can be generated by the aqueous purification of Pu, a means for removing Ga using a thermal technique has been investigated. This paper reports our laboratory scale studies of the kinetics of removal of Ga from gallia-doped ceria. CeO_{2-x} is a relatively good surrogate for PuO_{2-x} due to their many similar thermodynamic and physical properties [7–16]. Ceria is convenient to use compared with plutonia, for example, by eliminating the need to work in glove boxes and dispose radioactive waste, thereby saving money and time, and reducing worker exposure to radiation.

2. Experimental

CeO_2-based surrogates were prepared using a conventional route that involved blending, sintering, and milling CeO_2 and Ga_2O_3 powders. Table 1 lists the raw materials used in these studies. The primary surrogate of interest was CeO_2–2 wt% Ga_2O_3. After cerium oxide and gallium oxide powders were mixed, the mixture was vibration-milled for 15–20 min. The powder was then

* Corresponding author. Present address: US Department of Commerce, National Institute of Standards & Technologies, MS 8250, Gaithersburg 20899-0001, USA.

[1] Present address: Ceramatec, 2425 South 900 West, Salt Lake City, UT 841119, USA.

0022-3115/00/$ - see front matter
PII: S0022-3115(00)00064-7

Table 1
Description of the raw materials used to fabricate CeO_2–Ga_2O_3 surrogate powders

	Catalog name	Supplier	Description
Base powder	Gallium (III) oxide Ga_2O_3	Johnson Matthey	99.999%; −325 mesh
	Cerium (IV) oxide CeO_2	Johnson Matthey	99.99%; <5 μm
Binder	Polyethylene glycol (PEG)	J.T. Baker	PEG 8000 (U222-08)
	Stearic acid	E.M. Science	EM-SX0947-1
Lubricant	Liqui moly (MoS_2)	Lockery Company	Moly Grade NV; regular

pressed as a green pellet to 30–40% of theoretical density. The resulting pellet was again milled and sifted through a 100 mesh screen and pressed into a green pellet (60–70% of theoretical density). The pellets (0.6–0.7 cm O.D. and 1.0–1.2 cm height) were fired at 450°C for 4 h at a rate of 10°C/min to remove the binder. The pellets were subsequently heat-treated at 1650°C for 4 h in air (heating rate of 10°C/min), followed by a furnace cool. The average density of the sintered pellets (measured from 520 pellets) was above 95% of the theoretical density. After sintering, the sintered pellets were re-crushed into powders with desired particle sizes, typically – 100 mesh by either vibration or attrition milling.

Gallium was removed from the powder feedstock (and in some cases, whole pellets) by heat treating in high purity Ar–6% H_2 and, for comparison, pure Ar. Experiments were done by varying temperature (600–1600°C), time (0.5–12 h), sample size (0.3, 0.9, 2.5, 100 g), gas velocity (1.5–20 cm/s), and particle size (850–425, 425–250, 250–180, and −150 μm). Samples were placed in high-purity alumina crucibles, which in turn were placed in an alumina tube furnace. The samples were heated to the temperature of interest at nominally 20°C/min and cooled at the same rate. Specimen weights and gallium concentrations were measured before and after heat treatments. The amount of gallium oxide dissolved into the alumina crucible was determined to be negligible under all test conditions. A comparatively large surrogate sample (100 g) was heated at 1200°C for 12 h in Ar–6% H_2 flowing at 3 cm/s. Following the first exposure, the sample was well mixed and exposed a second time, and samples from each run were taken for analyses from the surface and inside of the powder pack regions, as discussed later. Test samples were analyzed by scanning electron microscopy (Joel 6300 FVX), energy dispersive X-ray analysis (EDS), X-ray photoelectron spectroscopy (XPS), direct current plasma emission spectroscopy (DCP), and the oxygen metal ratio was assessed using a Leco TC-136. The DCP measurement was used for quantitative analysis of gallium in the samples. Particle induced X-ray emission (PIXE), neutron activation analysis (NAA), and X-ray microfluorescence (XRMF) were also used to characterize the efficacy of Ga removal with sample lot sizes.

3. Results and discussion

3.1. Surrogate sample characterization

A nominal CeO_2–2 wt% Ga_2O_3 starting surrogate powder was vibration milled and sieved through a 100 mesh screen. Some particles were attrition milled. The volume average particle size was 76 μm for the vibration-milled and 1 μm for attrition-milled powder.

The weight loss during the sintering process was measured by non-isothermal thermogravimetric analysis (TGA) as shown in Fig. 1. The TGA trace showed a slightly larger weight loss for the processed surrogate than for pure CeO_2 when exposed to a N_2–20% O_2 environment. TGA traces showed slope changes for both samples near 1027°C that may be caused by transformation to non-stoichiometric $CeO_{1.78}$ at and above 1023°C [14]. The amount of Ga in the surrogate was reduced from *about* 14 100 to 7800 wppm after sintering *by DCP measurement.*

Fig. 2 shows an SEM microstructure and corresponding elemental maps of Ce and Ga of a cross-section of the sintered pellet. The microstructure shows pores and agglomerated grains formed during sintering. The X-ray elemental map of Ga shows strong Ga intensities at grain boundaries. The segregated Ga species were rarely observed within CeO_2 grains. The morphology of the sintered and crushed powder is shown in

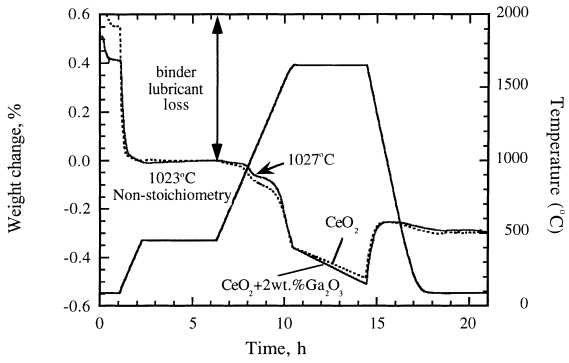

Fig. 1. TGA data for CeO_2 and CeO_2–2 wt% Ga_2O_3 surrogate pellets during sintering.

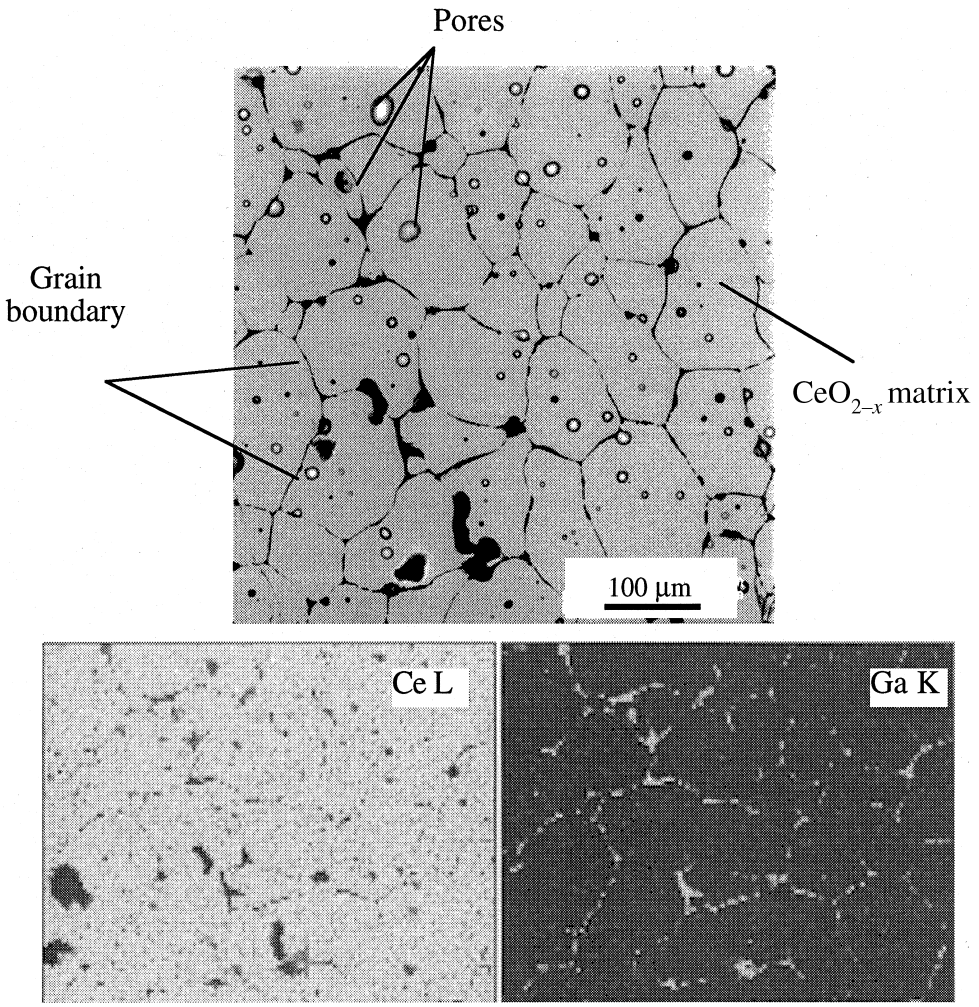

Fig. 2. SEM morphologies of the cross-section of the sintered pellet showing grain boundaries and pores through cross-section (top). X-ray elemental maps highlighting Ga segregation to the grain boundaries (bottom).

Fig. 3. The X-ray elemental map shows gallium-rich regions at grain boundaries within particles.

The gallium concentration changes during sintering (14100–7800 wppm) and SEM morphologies in Figs. 2 and 3 indicate that when gallia-doped ceria sintered, Ga_2O vaporizes from Ga_2O_3 in the powder and segregates to the grain boundaries. A portion of this gallium oxide in the grain boundaries is likely to form the $CeGaO_3$ perovskite phase when exposed in H_2 reducing conditions, as reported by previous investigators [7,13,17,18]. This phase is reduced more slowly than Ga_2O_3 and therefore may control the removal process at which the last few percent of Ga is removed. Therefore, the gallium-rich regions at the grain boundaries are still observed after exposing the pellet at 1200°C for 12 h to Ar–6% H_2, as shown in Fig. 4. Thus, it is possible that the efficiency of Ga removal through Ga_2O volatile species may depend on the extent of formation of the Ga-rich phases in the grain boundaries.

3.2. Thermally induced gallium removal

The results of weight change measurements taken on samples exposed to both Ar–6% H_2 and pure Ar for 30 min are shown in Fig. 5 as a function of sample geometry and temperature. The measured weight loss is the combined loss of Ga and O associated with the mass equations (1) and (2), by which the Ga_2O vapor pressure in the Ga_2O_3 are governed [19–21], as well as the loss of oxygen from cerium oxide, i.e., cerium oxide becomes more substoichiometric under reducing conditions [22,23]

$$Ga_2O_3(s) + 2H_2(g) = Ga_2O(g) + 2H_2O(g) \quad (1)$$

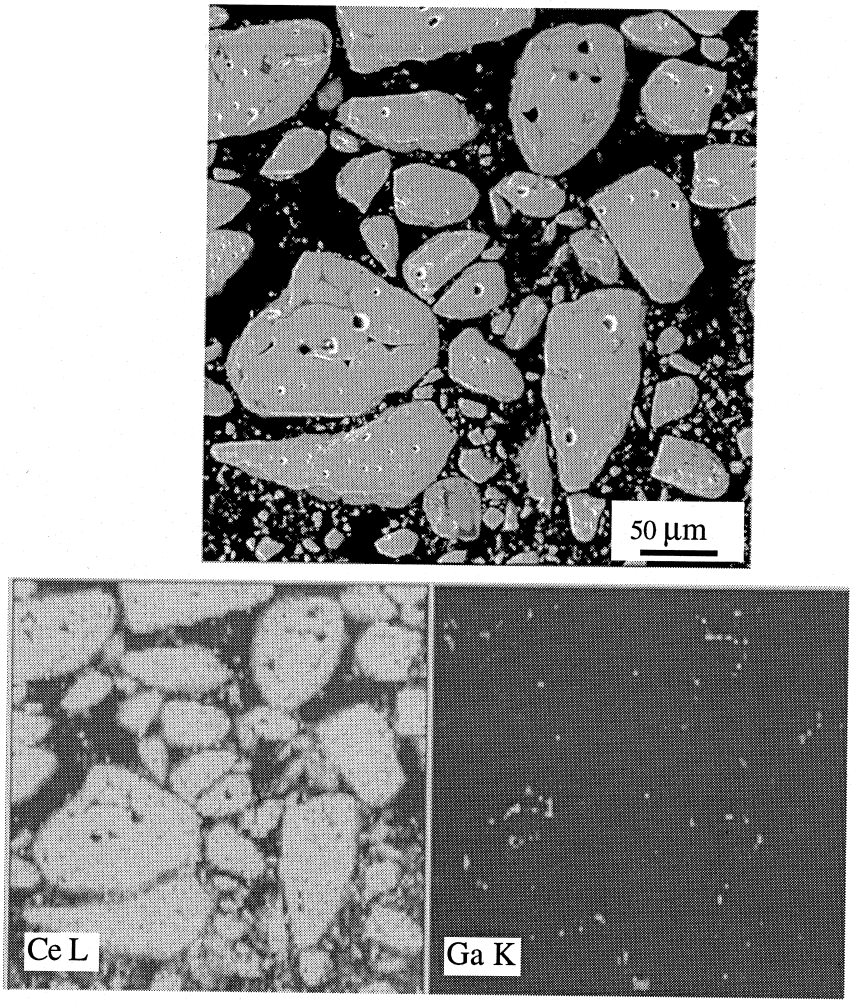

Fig. 3. SEM observations of CeO_2–2 wt% Ga_2O_3 powder crushed from pellets after sintering at 1650°C for 4 h. This crushed powder was used as a starting material for thermal treatment. Several grains are agglomerated in a particle (top). X-ray elemental maps (bottom) show gallium intense regions at the grain boundary in a particle.

$$Ga_2O_3(s) = Ga_2O(g) + O_2(g). \quad (2)$$

Therefore, weight loss alone is only a semi-qualitative measure of the gallium loss. As shown in Fig. 5, there is little or no weight change in Ar. The chemical analyses in Fig. 6 performed on samples exposed to Ar show no significant Ga loss, also in agreement with thermodynamic calculations in a previous publication [19]. Fig. 7 shows the residual amount of Ga as a function of temperature for surrogates exposed to Ar–6% H_2 for 30 min. As shown in Figs. 5–7, both mass and gallium losses observed in Ar–6% H_2 were significantly greater than that observed in Ar, particularly at higher temperatures. At 1000°C and above, the powder samples lost significantly more weight in Ar–6% H_2 than did the pellets. Figs. 5–7 verify that the kinetics of Ga removal are much higher at higher temperatures and in Ar–6% H_2. The residual amount of gallium after a much longer exposure time (4 h) is shown in Fig. 8, which also shows data obtained at temperatures above 1200°C. It is seen that gallium content can be lowered to 0.01–0.05% at a sufficiently high temperature and exposure time.

Fig. 9 shows the effect of time on the weight loss and residual Ga concentration in the samples exposed to Ar–6% H_2 for 0.5–12 h at 600°C, 900°C, and 1200°C. As exposure time increased, Ga continued to be removed, however at a lower rate. The residual Ga level reached 60–130 wppm in powder samples after 12 h at 1200°C. On the other hand, the pellets exposed to the same conditions contained approximately 2900 wppm Ga residue. Fig. 9 indicates that, in the early stage, the residual Ga species near the surface is reduced. In the later

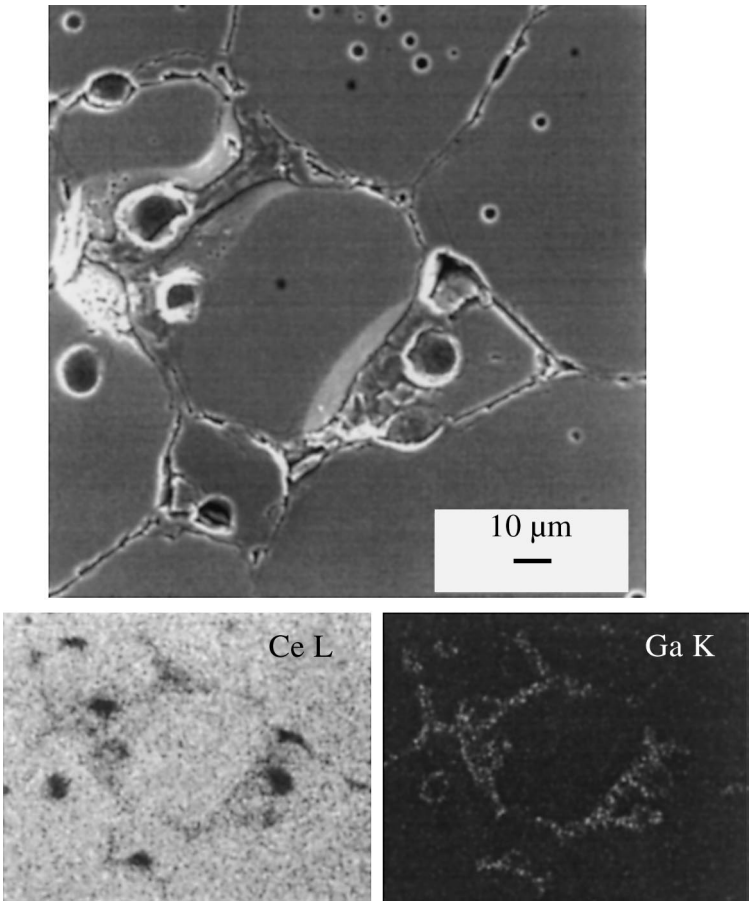

Fig. 4. SEM observations of CeO_2–2 wt% Ga_2O_3 powder surrogate exposed to Ar–6% H_2 at 1200°C for 12 h (top). X-ray elemental map (bottom) shows weaker Ga intensities at the grain boundaries than before thermal treatment as shown in Fig. 2.

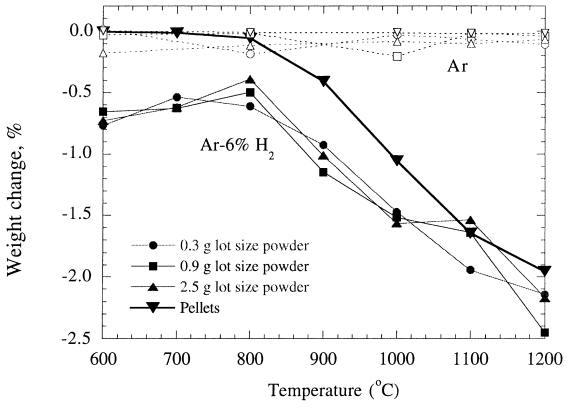

Fig. 5. Weight change versus temperature for CeO_2–2 wt% Ga_2O_3 surrogate samples exposed to Ar–6% H_2 and Ar for 30 min. Each point is the average of results from three runs.

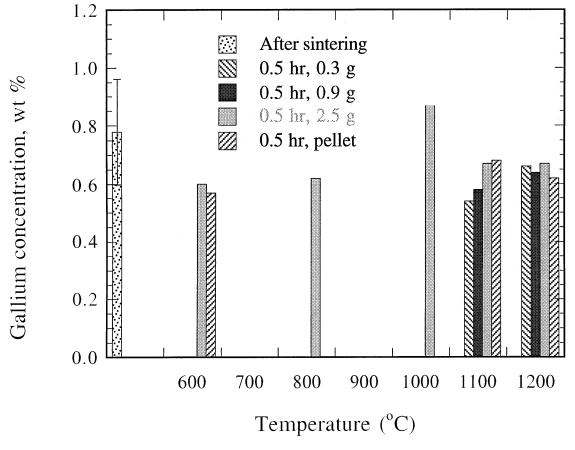

Fig. 6. Residual Ga versus temperature for CeO_2–2 wt% Ga_2O_3 samples exposed to Ar for 30 min.

stage, the removal may depend on the transport of Ga species, mainly $Ga_2O(g)$, from inside to outside of the surrogate resulting in the slower removal of Ga. In these, Figs. 6–9, it is seen that some samples heated at low temperatures and/or for short times, where the extent of gallium removal is low, contained higher contents

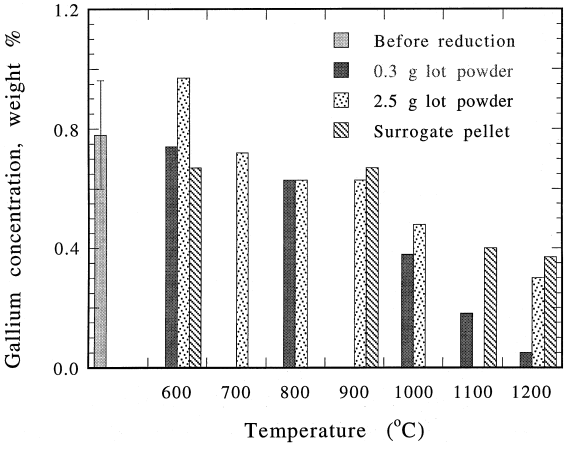

Fig. 7. Residual Ga versus temperature for CeO_2–2 wt% Ga_2O_3 samples exposed to Ar-6% H_2 for 30 min.

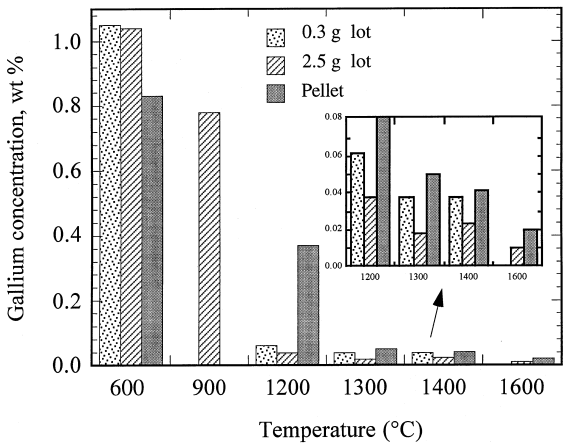

Fig. 8. Residual Ga for CeO_2–2 wt% Ga_2O_3 samples exposed to Ar–6% H_2 for 4 h and at higher temperatures.

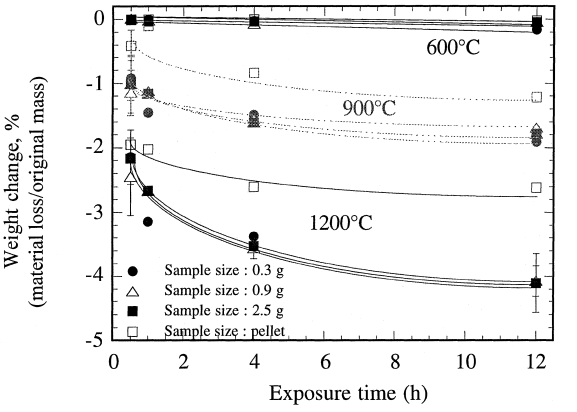

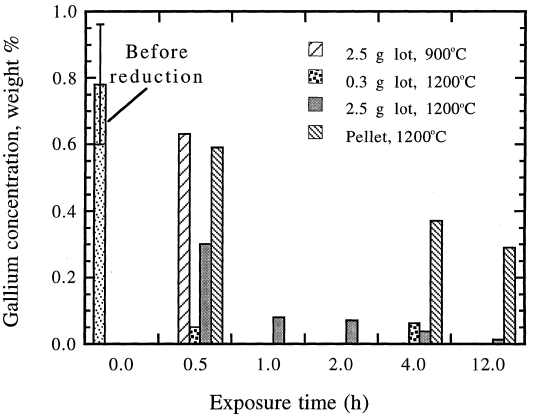

Fig. 9. Weight loss (above) and residual Ga (bottom) versus time for CeO_2–2 wt% Ga_2O_3 samples exposed to Ar–6% H_2 at 900°C and 1200°C.

of gallium than the starting material. This is due to the non-uniform distribution of gallium in the latter and/or the uncertainty of gallium analysis. Thus, this variation represents the overall degree of uncertainty of data presented in this work.

Fig. 10 shows the effect of sample size on the Ga removal at 1200°C for CeO_2–2 wt% Ga_2O_3 exposed to Ar–6% H_2 for 30 min determined by XPS, PIXE, and DCP analyses. Other techniques such as NAA and XRMF showed the same trend as highlighted in Fig. 10; i.e., that the efficacy of Ga removal observed with decreasing sample lot size at 1200°C [20,24].

Fig. 11 summarizes the results of Ga removal experiments performed on a 100 g sample of surrogate powder at 1200°C for 12 h in Ar–6% H_2 flowing at 3 cm/s. Following the first exposure, the sample was thoroughly mixed in a mixer. After mixing, the powder was packed in the crucible and heated a second time. Samples were taken after both runs from three upper positions near the surface, two lower positions, and after mixing the entire sample as indicated in Fig. 11. After the first run, gallium concentration near the surface of the bed was lower than inside of the powder pack. This suggests that the vaporization of gallium from the surrogate is influenced by the gaseous transport of Ga_2O. However, after the second run, the gallium concentration at the upper surface of the bed is not much different from the inside of the powder pack. This suggests that the removal of the gallium remaining after the first run is slower, possibly controlled by the solid-state diffusion within the grains.

Fig. 12 shows the effect of the gas flow rate on Ga removal. The upper plot in Fig. 12 shows weight changes with flow rates of 1.5 and 3.0 cm/s from 600°C to 1200°C, and lower one is the weight changes with flow rates of 1.5–6.0 cm/s at 1200°C. The shaded regions in Fig. 12 show the hypothetical mass loss for samples exposed at 3.0 cm/s, assuming that the gallium and

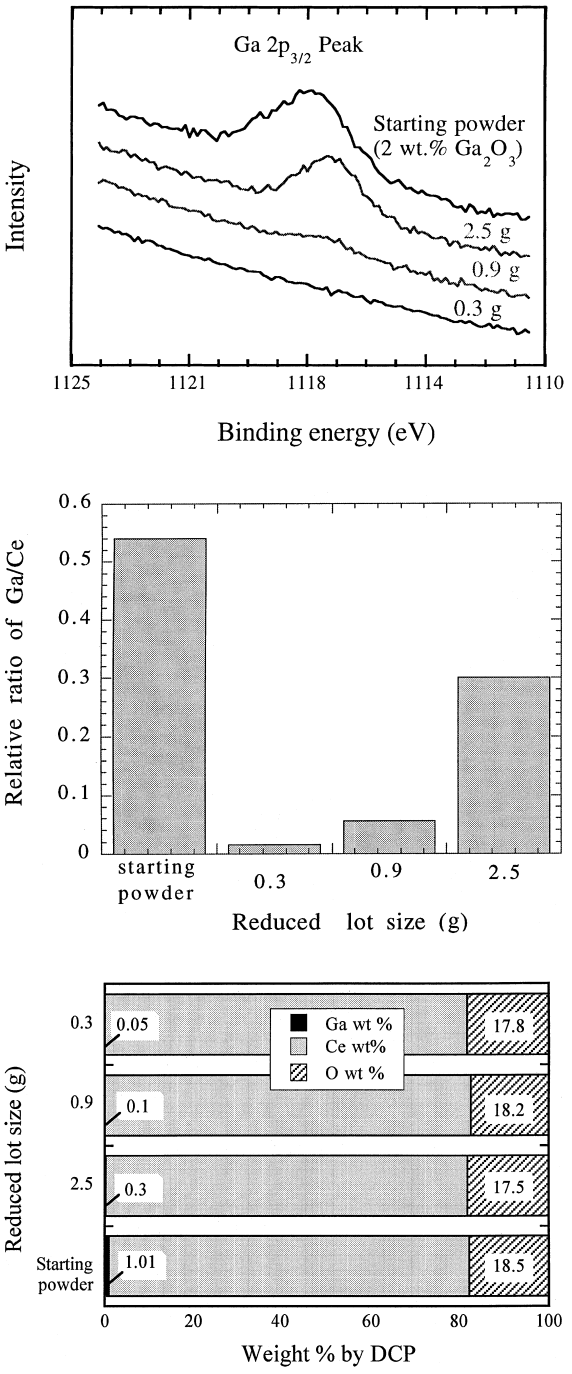

Fig. 10. Ga removal versus sample lot size, showing greater degrees of Ga removal from smaller sample lots at 1200°C. Samples were exposed to Ar–6% H_2 for 30 min, and analyzed by XPS (top), PIXE (middle) and DCP (bottom).

oxygen fluxes increase as the square root of gas velocity based on gaseous diffusion control. However, the experimental weight losses do not exhibit a linear dependency on square root of gas velocity. The residual gallium analysis data also showed no dependency with respect to flow rates. This implies that the kinetics are not limited by gaseous diffusion in H_2 through the extended boundary layer in the range of 1.5–6.0 cm/s. We performed experiments with 20 cm/s flow rate, which also showed no effect on the gallium removal. However, this result does not preclude the possibility that Ga_2O gaseous transport through the inter-particle pores is the rate limiting or partially rate limiting, as discussed later.

The effect of particle size shown in Fig. 13 indicates a general trend of increasing Ga removal rate with decreasing size, although some inconsistencies are present, especially for the two largest size fractions. The attrition-milled powder (average size of 1 μm; single point at 1200°C) had a considerably higher degree of removal than the larger particles.

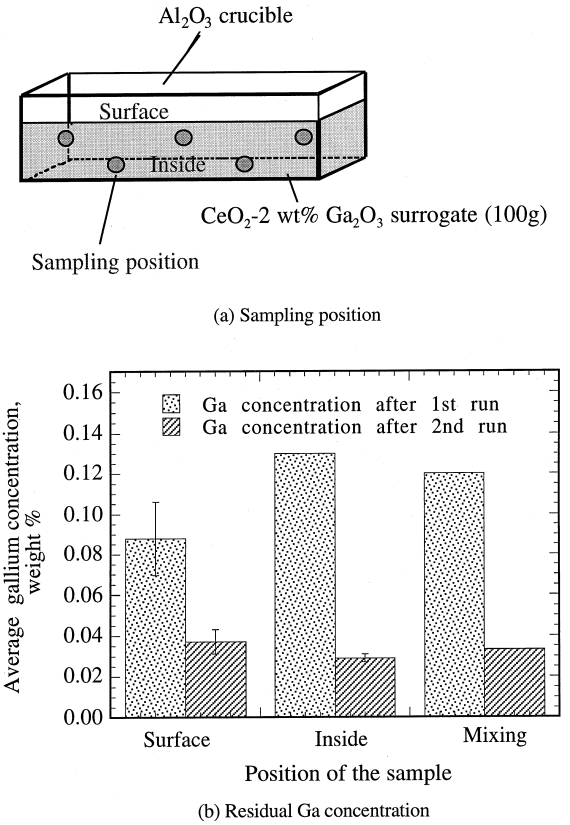

Fig. 11. Residual Ga amount from 100 g lot size powder sample after reaction at 1200°C for 12 h in Ar–6% H_2 (Gallium concentration was averaged from three measurements for the surface sample and from two measurements for the inside sample. A single measurement was made for the mixture sample. The results of the two measurements for the inside sample after the first run were so close that the error bar is almost invisible).

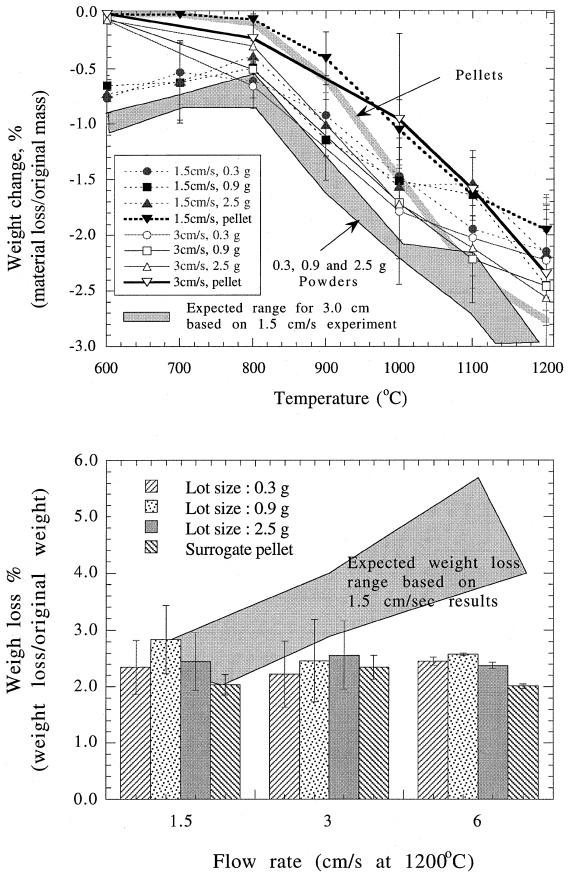

Fig. 12. The effect of gas flow rate on Ga removal for CeO_2–2 wt% Ga_2O_3 samples exposed to Ar–6% H_2 with flow rates of 1.5 and 3.0 cm/s for various temperatures and lot sizes (top), and with flow rates of 1.5–6.0 cm/s at 1200°C (bottom).

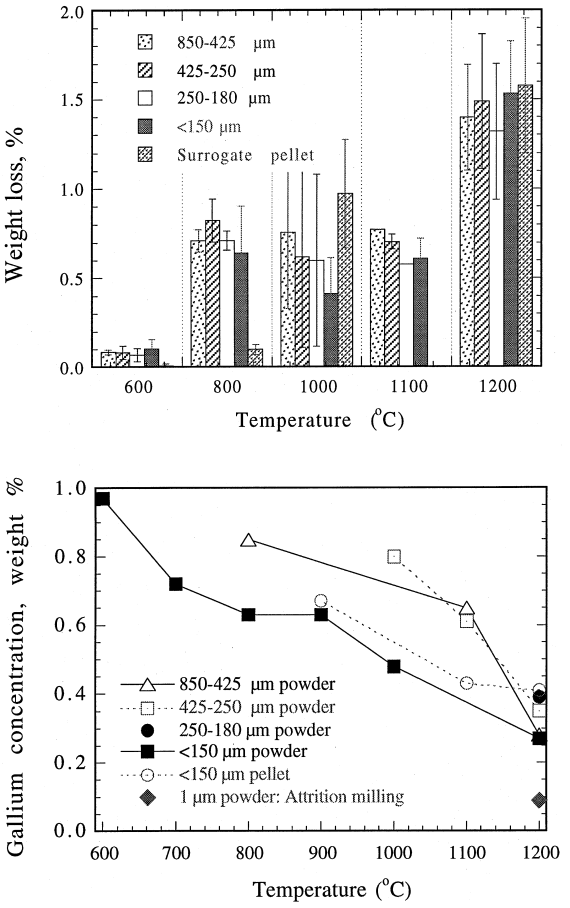

Fig. 13. Particle size effects on the weight loss (above) and Ga concentration (bottom) versus temperature for 2.5 g of CeO_2–2 wt% Ga_2O_3 exposed to Ar–6% H_2 for 1 h removal process.

3.3. Kinetics and rate-controlling step for Ga removal

The possible mechanisms of Ga removal are illustrated in Fig. 14. The possible rate controlling steps for Ga removal are (1) the external mass transfer between bulk gas phase and the surface of a particle or pellet, (2) chemical reaction at the surface of the surrogate, (3) transport of Ga species from within the particle or pellet to the surface, and (4) for a loose pack of powder or a porous pellet, the diffusion of $Ga_2O(g)$ and $H_2(g)$ in the particle interstices or pores.

Although Ga_2O_3 could possibly decompose to Ga(l), GaOH(g), GaO(g), and $Ga_2O(g)$, the main volatile species is $Ga_2O(g)$ in a H_2 environment [19]. These possible decomposition products have been reported by thermodynamic analysis and physical measurements by other researchers [4,16,19].

The rate of mass transfer through the gas phase boundary layer is described by the following equations [25,26]:

$$\dot{m}_{Ga_2O_3} = hA\Delta P \tag{3}$$

with

$$h \propto D^{2/3}\gamma^{-1/6}\left(\frac{v}{L}\right)^{1/2}, \tag{4}$$

where h is the mass transfer coefficient, A the surface area, D the diffusion coefficient of Ga_2O in H_2, γ the kinematic viscosity of the gas mixture, v the bulk gas stream velocity, L the length of the specimen, and ΔP is the difference in the partial pressures of Ga_2O between the bulk gas and that at the surface of the specimen. Because we used the same geometry and conditions in all the surrogate samples, the kinematic viscosity of the gas mixture and the length of the specimen were unchanged. As shown in Eqs. (3) and (4), mass flux should be proportional to the square root of the gas velocity for a rate controlling step (1). As already shown in Fig. 12, the weight loss in the surrogate did not depend on the flow rate. Thus, step (1) cannot be the rate-controlling step in

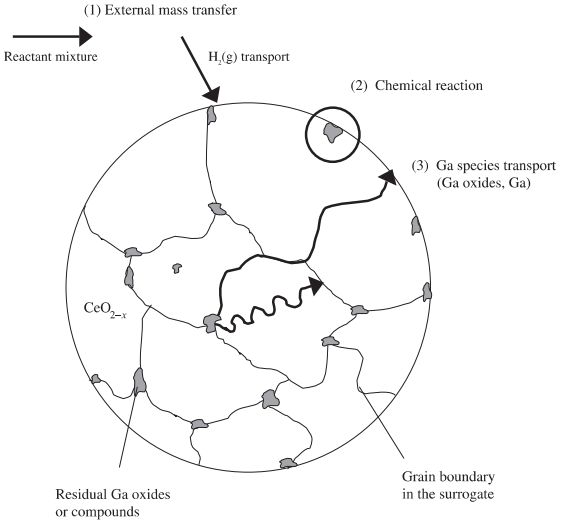

Fig. 14. Possible mechanisms of gallium removal in the MOX surrogate during the thermal removal process.

the whole process of gallium removal from the surrogate within the flow rate range tested.

The dependence of gallium removal rate on powder lot size, seen in Figs. 7–11 together with that on particle size shown in Fig. 13 suggests that the rate controlling step in this system is a combination of steps (3) and (4).

For a non-porous particle or piece of sample, the rate of Ga removal can be obtained based on the equations describing the solid-state diffusion of gallium oxide, given by

$$D^{s}_{Ga}\nabla^2 C_{Ga} = \frac{\partial C_{Ga}}{\partial t} \tag{5}$$

with

$$\text{at } t = 0, \quad C_{Ga} = C^{i}_{Ga}, \tag{6}$$

at particle surface

$$-D^{s}_{Ga}\frac{\partial C_{Ga}}{\partial r} = 2h(p_{Ga_2O} - p^{b}_{Ga_2O}), \tag{7}$$

at particle center

$$\frac{\partial C_{Ga}}{\partial r} = 0, \tag{8}$$

where D_{Ga} is the solid-state diffusivity of Ga, C_{Ga} the Ga concentration in the solid phase, h the mass transfer coefficient, r the radial coordinate in the particle, t the time, and p is Ga_2O partial pressure in the gas phase. The superscripts i in Eq. (6) and b in Eq. (7) denote the initial and bulk values, respectively.

The gallium removal rate from a particle is given by

$$\dot{m}_{Ga} = -D^{s}_{Ga}A\left.\frac{\partial C_{Ga}}{\partial r}\right|_{r=R}, \tag{9}$$

where $\dot{m}_{Ga}$ is the Ga removal rate and A is the surface area. In the case of rapid external mass transfer and zero Ga_2O partial pressure in the bulk gas stream, the solution to Eqs. (5)–(8) for a spherical particle is

$$\frac{C_{Ga}}{C^{i}_{Ga}} = 2\sum_{n=1}^{\infty}(-1)^{n+1}(e^{-\lambda_n D_{Ga} t})\frac{\sin\lambda_n r}{\lambda_n r}, \quad \lambda_n = \frac{n\pi}{R}. \tag{10}$$

For a porous pellet or a loose pack, consisting of small non-porous grains, the gas-phase diffusion of Ga_2O and H_2 in the pores must be considered as follows:

$$D^{e}_{Ga_2O}\nabla^2 p_{Ga_2O} + \frac{RT}{2}R_{Ga} = \varepsilon\frac{\partial p_{Ga_2O}}{\partial t} \cong 0, \tag{11}$$

$$D^{e}_{H_2}\nabla^2 p_{H_2} - \frac{RT}{2}(-R_{H_2}) = \varepsilon\frac{\partial p_{H_2}}{\partial t} \cong 0. \tag{12}$$

Appropriate boundary conditions similar in form to those of Eqs. (7) and (8) apply to Eqs. (11) and (12). Here, $D^{e}_{Ga_2O}$ and $D^{e}_{H_2}$ represent, respectively, effective Ga_2O and H_2 diffusion coefficient in the pores. R_{Ga} represents the local molar rate of gallium evolution per unit volume of the pellet, which can be obtained by solving Eqs. (5)–(9). $(-R_{H_2})$ represents the local molar rate of consumption of H_2 per unit pellet volume by reaction with Ga_2O_3 as well as the host oxide, ceria. Eqs. (5)–(12) are given here as possible model equations for a more quantitative further investigation of the problem discussed in this paper. Such a study was beyond the scope of the present work. It has been reported that the solubilities of Ga in cerium and plutonium are similar [7,13]; thus Pu-based MOX fuel is expected to have similar kinetics as gallia-doped ceria surrogate discussed here.

4. Conclusions

Gallium removal from cerium oxide, as a surrogate of plutonium oxide, was investigated to determine the effects of atmosphere, temperature, particle size, sample lot size, exposure time, and gas flow rate. The presence of hydrogen and temperature had strong effects on Ga removal. Results to date suggest that the gallium level in the surrogate powder can be reduced to levels as low as 60–100 wppm from the starting ceria doped with gallia powder.

Gallium removal from the surrogate is achieved by the reduction of Ga_2O_3 in hydrogen, which produces volatile Ga_2O. The results show that the mechanism of gallium removal involves several steps. The removal of gallium from the ceria may depend on the reduction

of segregated gallium oxide species in the grain boundaries. At the beginning of gallium removal process, the vaporization of gallium oxide and Ga_2O transport from the surface may be the dominant mechanism, but after the depletion of gallium near the surface, the diffusion of gallium species plays an important role in the subsequent stage to remove the residual gallium.

Acknowledgements

This work was supported by the US Department of Energy. The authors are grateful to Hisham Ziraffe and Arlette Antencio for assisting in the fabrication of surrogate specimens during their summer internships at Los Alamos National Laboratory. The authors are also very grateful for helpful discussions with Dr David Kolman, Dr Reed Jensen and Dr John Buksa of Los Alamos National Laboratory.

References

[1] Department of Energy, Plutonium focus area – technology summary, US Department of Energy Report DOE/EM-0297, 1996.
[2] National Academy of Science, Management and disposition of excess weapons plutonium, National Academy, Washington, DC, 1995.
[3] Department of Energy, Surplus plutoium desposition darft environmental impact statement, DOE/EIS-0283-D, July 1998.
[4] D.F. Wilson, E.C. Beahm, T.M. Besmann, J.H. Devan, J.R. Distefano, U. Gat, S.R. Greene, P.L. Rittenhouse, B.A. Worley, Potential effects of gallium on cladding materials, Oak Ridge National Laboratory Report ORNL/TM-13504, 1997.
[5] US Department of Energy, Program acquisition strategy for obtaining mixed oxide (MOX) fuel fabrication and reactor irradiation service (PAS) workshop, Office of Fissile Materials Disposition and Chicago Operations Office, 28 August 1997.
[6] D.F. Wilson, J.R. Distefano, J.F. King, E.T. Manneschmidt, J.P. Strizak, Interactions of zircaloy cladding with gallium, 1997 Status, Oak Ridge National Laboratory Report ORNL/TM-13505, 1997.
[7] P.R. Luebber, W.F. Michayd, O.K. Chopra, Compatibility of ITER candidate structural materials with static gallium, Argonne National Laboratory Report ANL-93/31, 1993.
[8] T.B. Lindemer, Assessment of gallium effects in processing and performance of U–Pu Oxide LWR fuels, Oak Ridge National Laboratory Report ORNL/MD/LTR-38, 1995.
[9] D.R. Lide, Handbook of Chemistry and Physics, 77th Ed., CRC, New York, 1996–1997.
[10] L.R. Morss, J. Fuger, Transuranium Elements, American Chemical Society, Washington, DC, 1992.
[11] A. Nakamura, J. Nucl. Mater. 201 (1993) 17.
[12] O. Toffsørensen, J. Solid-State Chem. 18 (1976) 217.
[13] C. Guminski, Z. Metallkd. 81 (1990) 105.
[14] Per Kofstad, Nonstoichiometry, Diffusion, and Electrical Conductivity in Binary Metal Oxides, vol. 276, Wiley-Interscience, New York, 1972.
[15] J.L. Smith, Z. Fisk, S.S. Hecker, Physica B 130 (1985) 151.
[16] G.V. Samsonov, The Oxide Handbook, IFI/Plenum Data Corporation, New York, 1973.
[17] M.L. Keith, R. Roy, Amer. Mineralogist 39 (1954) 1.
[18] A.L. Leonov, A.V. Andreeva, V.E. Shvaiko, K. Keler, Neorg. Mater. 2 (3) (1996) 517.
[19] D.P. Butt, Y.S. Park, T.N. Taylor, J. Nucl. Mater. 264 (1998) 71.
[20] Y.S. Park, T.N. Taylor, A. Antencio, D.P. Butt, Environmental Issues and Waste Management Technologies in the Ceramic and Nuclear Industries IV, Ceramic Transactions 69, American Ceramic Society, 1998.
[21] T.M. Besmann, J. Am. Ceram. Soc. 81 (12) (1998) 3071.
[22] A. Laachir, V. Perrichon, A. Badri, J. Lamontte, E. Catherine, J.C. Lavalley, J.E. Fallah, L. Hilaire, F.I. Normand, E. Quêmêrê, G.N. Sauvion, O. Touret, J. Chem. Soc. Faraday Trans. 87 (10) (1991) 1601.
[23] M. Romeo, K. Bak, J.E. Fallah, F.L. Normand, L. Hilaire, Surf. Interf. Anal. 20 (1993) 508.
[24] Y.S. Park, D.G. Kolman, H. Ziraffe, C.L. Haertling, D.P. Butt, in: Scientific Basis for Nuclear Waste Management XXII, Mater. Res. Soc. Proc. vol. 556, Materials Research Society, 1999, p. 129.
[25] Geiger, Poirier, Transport Phenomena in Metallurgy, Addison-Wesley, Reading, MA, 1973.
[26] R.B. Bird, W.E. Stewart, E.N. Lightfoot, Transport Phenomena, Wiley, New York, 1960.